Articles

Characterization of Subunit-Specific Interactions in a Double-Stranded RNA Virus: Raman Difference Spectroscopy of the φ6 Procapsid†

James M. Benevides,‡ Jarmo T. Juuti,§ Roman Tuma,§ Dennis H. Bamford,§ and George J. Thomas, Jr.*,‡

Division of Cell Biology and Biophysics, School of Biological Sciences, University of Missouri-Kansas City, Kansas City, Missouri 64110, and Department of Biosciences and Institute of Biotechnology, University of Helsinki, 00014 Helsinki, Finland

Received February 25, 2002

ABSTRACT: The icosahedral core of a double-stranded (ds) RNA virus hosts RNA-dependent polymerase activity and provides the molecular machinery for RNA packaging. The stringent requirements of dsRNA metabolism may explain the similarities observed in core architecture among a broad spectrum of dsRNA viruses, from the mammalian rotaviruses to the *Pseudomonas* bacteriophage φ6. Although the structure of the assembled core has been described in atomic detail for *Reoviridae* (blue tongue virus and reovirus), the molecular mechanism of assembly has not been characterized in terms of conformational changes and key interactions of protein constituents. In the present study, we address such questions through the application of Raman spectroscopy to an in vitro core assembly system—the procapsid of φ6. The φ6 procapsid, which comprises multiple copies of viral proteins P1 (copy number 120), P2 (12), P4 (72), and P7 (60), represents a precursor of the core that is devoid of RNA. Raman signatures of the procapsid, its purified recombinant core protein components, and purified sub-assemblies lacking either one or two of the protein components have been obtained and interpreted. The major procapsid protein (P1), which forms the skeletal frame of the core, is an elongated and monomeric molecule of high α-helical content. The fold of the core RNA polymerase (P2) is also mostly α-helical. On the other hand, the folds of both the procapsid accessory protein (P7) and RNA-packaging ATPase (P4) are of the α/β type. Raman difference spectra show that conformational changes occur upon interaction of P1 with either P4 or P7 in the procapsid. These changes involve substantial ordering of the polypeptide backbone. Conversely, conformations of procapsid subunits are not significantly affected by interactions with P2. An assembly model is proposed in which P1 induces α-helix in P4 during formation of the nucleation complex. Subsequently, the partially disordered P7 subunit is folded within the context of the procapsid shell.

Most double-stranded (ds) RNA viruses share similar genetic and structural features, including a segmented linear genome packaged within an icosahedral capsid. Generally, the innermost component of the mature virion is an RNA polymerase complex that is formed from multiple copies of a small number of virally encoded proteins (*1*−*4*). The polymerase complex carries out the essential functions of RNA packaging, replication, and transcription within the host cell (*5*). Recent atomic models of the core assemblies of blue tongue virus (BTV) and reovirus provide insight into the structure of the polymerase complex (*1*, *4*). In both cases the inner shell is formed from 60 asymmetric dimers of the major structural protein (VP3 in BTV, λ1 in reovirus), which are arranged on a $T = 1$ icosahedral lattice. For reovirus, a part of the RNA processing machinery has been resolved at the 5-fold vertexes of the lattice (*4*), but no structural information is available for the replication−transcription machinery. An assembly mechanism proposed on the basis of the high-resolution structure of BTV suggests that the major structural protein (VP3) associates initially into decamers, which subsequently polymerize to form the core (*1*). However, the unavailability of an in vitro assembly system and the absence of soluble structural proteins for BTV and other dsRNA animal viruses preclude further experimental verification and characterization of conformational changes during assembly. On the other hand, a complete in

† Support from the U. S. National Institutes of Health (Grant GM 50776 to GJT), the Academy of Finland (Grant 168694 to D.H.B. and 172623 to R.T.), and the Finnish Center of Excellence Program 2000-2005 (SA164298) is gratefully acknowledged. This is paper LXXXI in the series Studies of Virus Structure by Raman Spectroscopy.

* To whom correspondence may be addressed. Email: thomasgj@umkc.edu. Tel: 816-235-5247. Fax: 816-235-1503.

‡ University of Missouri-Kansas City.

§ University of Helsinki.

[1] Abbreviations: L-, M- and S−RNA, large, medium and small segments of the dsRNA genome of φ6; BTV, blue tongue virus; dsRNA, double-stranded RNA; cryo-EM, electron cryomicroscopy; PC, procapsid; SDS−PAGE, sodium dodecyl sulfate polyacrylamide gel electrophoresis.

10.1021/bi0201623 CCC: $22.00
Published on Web 09/10/2002

Table 1: Plasmids and Protein Products

plasmid	host	protein product	ref
pAP6	JM109	P127 particle	*23*
pEM2	BL21(DE3)	P2 protein	*24*
pJTJ7	HMS174(DE3)	P4 protein	*42*
pJTJ12	HMS174(DE3)	P7 protein	*8*
pLM358	JM109	P14 particle	*15*
pLM450	JM109	procapsid	*15*
pLM574	JM109	P124 particle	*15*
pLM609	JM109	P147 particle	*15*
pLM1224	JM109	procapsid deficient in P4	*23*

vitro assembly and replication system is available for the bacteriophage φ6 (*6*), which is recognized as a model for the assembly and replication of dsRNA viruses (*3*, *7*−*9*).

The φ6 virion is a complex triple-layered icosahedral phage infecting *Pseudomonas syringae*. The outermost layer is a lipid envelope carrying the receptor-binding spike that is utilized during the membrane fusion event of the cell entry process (*10*, *11*). The intermediate layer is composed of a single protein species (P8) forming a $T = 13$ surface lattice (*7*). This layer protects the core when the nonenveloped particle crosses the plasma membrane (*12*, *13*). The innermost core particle is composed of four protein species (copy number): P1 (120), P2 (12), P4 (72), and P7 (60). The 120 copies of P1 form the core dodecahedral framework (a $T = 1$ lattice, triangulated with dimers). Each 5-fold vertex contains a P4 hexamer (*14*). Upon the basis of symmetry considerations, it is assumed that one P2 subunit (the RNA-dependent RNA polymerase) is also present at each 5-fold vertex. Similarly, the stoichiometry of P7 (30 dimers) suggests localization at the 2-fold symmetry positions.

Expression of recombinant forms of the core proteins leads to the formation of empty precursor particles (procapsids) having the same protein composition as the viral core, although all subunits do not have the same conformations exhibited in the core (*7*, *14*, *15*). Using appropriate gene constructs, both incomplete procapsids and purified recombinant proteins P2, P4, and P7 can also be produced (Table 1). Recently, we demonstrated that the purified recombinant P2 monomer is competent for incorporation into capsids (*6*). In vitro reconstitutions from the purified recombinant proteins yield procapsids with biological properties that are indistinguishable from activities of their cell-derived counterparts: viz. the ability to package genomic ssRNA precursors, synthesize minus-strand RNA within the particle, and produce plus-strand transcripts. In addition, the recombinant particles can be rendered infectious by assembling a shell of protein P8 around them (*6*). Thus, the φ6 system represents a model that is well suited to probing kinetic and structural determinants of dsRNA virus assembly.

In the present work, we employ Raman difference spectroscopy to investigate conformations of the protein building blocks of the φ6 viral core particle. Conformational changes resulting from specific interactions within the core are identified. The Raman difference method is well established as a sensitive probe of structural changes that occur during virus assembly (*16*), and recent applications have provided structural information on both precursor and mature states of assembled viral subunits (*13*, *17*−*20*). The present application extends the methodology to the more complex polymerase machinery of a dsRNA viral procapsid. The specific φ6 constructs and constituent proteins examined here are listed in Table 2. By use of sensitive Raman difference methods, we demonstrate that φ6 procapsid assembly is accompanied by substantial and highly localized conformational changes among the interacting subunits. The results complement previously reported kinetic determinants of the φ6 in vitro assembly model (*6*).

Table 2: Nomenclature for Samples Investigated by Raman Spectroscopy[a]

sample	description
PC	procapsid assembled from recombinant P1, P2, P4, and P7 proteins
P124	PC-like particle lacking P7 protein
P127	PC-like particle lacking P4 protein
P147	PC-like particle lacking P2 protein
P14	PC-like particle lacking P2 and P7 proteins
PC^{LM1601}	PC (from pLM1224);[a] partially deficient in P4 protein
P1	purified recombinant P1 protein (monomer)
$P1^{agg}$	aggregated recombinant P1 protein (dodecahedral assembly)
P2	purified recombinant P2 protein (monomer)
P2′	procapsid-incorporated P2 protein; obtained by spectral subtraction
P4	purified recombinant P4 protein (hexamer)
P4′	procapsid-incorporated P4 hexamer; obtained by spectral subtraction
P7	purified recombinant P7 protein (dimer)
P7′	procapsid-incorporated P7 protein; obtained by spectral subtraction

[a] See also Table 1 for additional nomenclature.

MATERIALS AND METHODS

Reagents. Chemicals used in buffer and media preparations were of the standard reagent grades available from commercial suppliers. RNase A was obtained from Sigma (St. Louis, MO).

Preparation of Subviral Particles and Proteins. Incomplete procapsid-like particles (Table 1) were produced as described previously (*21*) with the following modifications: A booster culture of Luria-Bertami broth (50 mL) was inoculated and grown at 28 °C for 24 h and diluted into 500 mL of fresh media. Cells were further grown at 22 °C to a density of ∼2 × 10^8 mL^{-1} and then induced with 1 mM isopropylthiogalactose. Cells were harvested 14 h post induction by centrifugation and resuspended in 6−7 mL of 20 mM Tris buffer, pH 8, and lysed using a French pressure cell. The lysate was extracted twice with Triton TX-114 and loaded onto a 5−20% w/v sucrose gradient (Beckmann SW28 rotor, 24 000 rpm, 10 °C, 130 min). The particles in the collected bands (1.5−3 mL from each tube) were pelleted in a Beckmann Ti50.2 rotor (40 000 rpm, 10 °C, 90 min). The supernatant was removed, and the tubes were rinsed quickly with deionized water. Pellets were used immediately for preparing samples for Raman analysis and were kept on ice at all times. Buffer contributions were compensated by standard spectral subtraction methods (*22*).

Monomeric P1 was obtained from the P14 (Table 2) particles by three cycles of freeze−thawing in high salt buffer (20 mM Tris, 0.5 M NaCl, pH 8.1) containing 14% sucrose, as previously described (*6*). The dissociation was followed by size-exclusion chromatography using Superdex 200 media (Pharmacia, Uppsala, Sweden). P1 was concentrated to 4 μg/μL. (At higher concentrations extensive aggregation of P1

was observed.) Residual aggregates were removed from the concentrated P1 solution by centrifugation and the sample analyzed on an analytical Sephadex 200 size-exclusion column. The sample contained mostly monomer (90%) with modest amounts of oligomer present. The P1 inclusion body aggregate ($P1^{cage}$) was prepared using bacterial strain HMS174-(DE3) harboring the plasmid pEM1 (gift of E. Makeyev). Expression of P1 usually resulted in the formation of insoluble spherical particles (*23*). Such aggregates were washed with a salt solution (0.5 M NaCl) and treated with RNase and DNase to remove nucleic acids. These aggregates were further purified using 1% Triton X-100 to remove membrane fragments and pelleted through a 20% sucrose cushion. The pellet was resuspended in 20 mM Tris, 0.5 M NaCl, pH 8.1.

Protein P2 was expressed in *E. coli* at low temperature (23 °C) and purified using an established protocol (*24*). Production and purification of recombinant proteins P4 and P7 were carried out according to previously described protocols (*8*, *25*).

Monodispersity and oligomeric and hydrodynamic properties of the purified proteins were determined using a size-exclusion column (Superdex 200, 30 × 1 cm, Pharmacia, Uppsala, Sweden) coupled to a light scattering instrument and correlator (PDI 2020, Precision Detectors, Inc, Franklin, MA), as previously described (*26*).

Raman Spectroscopy. Solutions of proteins and pellets of protein assemblies, prepared as detailed above, were sealed in Kimax glass capillaries (No. 34504) for spectroscopic examinations. All samples were thermostated at 10 °C during data collection protocols and checked for integrity and activity after data collection. Limits of spectral reproducibility were established by comparison of several data sets collected from independently prepared samples. Raman spectra were excited with the 514.5 nm line of an argon laser (Coherent Inc. model Innova 70) using approximately 200 mW of radiant power at the sample. Raman scattering was collected in the 90° geometry and analyzed using a triple spectrograph (SPEX model 1877) equipped with a liquid nitrogen cooled charge-coupled device detector (Princeton Instruments model ST130). Typically, two exposures of 120 s each were accumulated, and 15 such accumulations were averaged to produce spectra shown in the figures below. The effective spectral resolution was 5 cm^{-1} and reported Raman frequencies are accurate to ±1 cm^{-1} for sharp bands and ±2 cm^{-1} or more for broad bands. The Raman spectrum of each sample was corrected for contributions of the buffer using standard procedures (*22*). A previously described, least-squares protocol was used to generate difference spectra by minimization of the resultant spectral changes (*27*−*29*). Raman difference peaks and troughs that represent at least 4% of the parent band intensity and have a signal:noise ratio of at least 2:1 are judged to be experimentally significant. Further details of sample handling and data analysis for Raman spectroscopy are given elsewhere (*27*, *28*).

RESULTS

Characterization of Subviral Particles by Raman Spectroscopy. Although reliable procedures have been established for in vitro production of φ6 procapsids and procapsid-like particles, incomplete incorporation or partial loss of one or more protein components may occur (*8*, *21*). Therefore, it is appropriate to assess whether protein compositions of the PC and PC-like particles examined here correspond to those of the native polymerase complex. The samples employed in this study were characterized by gel electrophoresis. The results, shown in Figure 1, confirm that protein compositions are equivalent stoichiometrically to those of the polymerase complex.

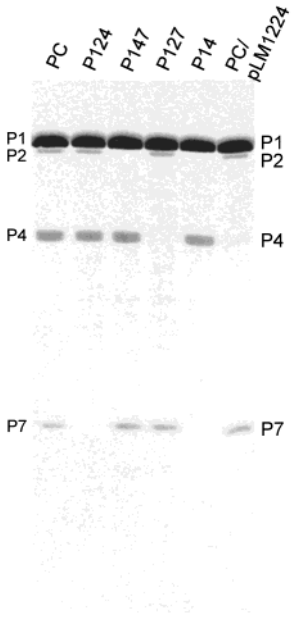

FIGURE 1: Coomassie-stained SDS−PAGE (15%) assays of the φ6 procapsid (PC) and procapsid-like particles.

Particles of the polymerase complex for which Raman spectra have been obtained, and the spectral subtraction schemes employed to simulate Raman signatures of the PC constituents, are summarized in Table 2. These spectra serve as the basis for computing the Raman signatures that correspond to procapsid-incorporated states of P1, P2, P4, and P7, as discussed below.

Assembly of P1. Protein P1 was purified as a monodisperse monomer (85 kDa) exhibiting a hydrodynamic radius of 3.8 ± 0.4 nm (*6*). Raman spectra were obtained from a dilute solution (∼4 μg/μL) of the monomer (Figure 2, trace B). The Raman bands diagnostic of protein secondary structure are amide I at 1654 cm^{-1}, amide III at 1251 cm^{-1}, and a main chain mode at 1340 cm^{-1}. These spectral markers indicate that the fold of P1 is predominantly α-helical. The high α-helical content of P1 is further supported by the prominent Raman marker at 939 cm^{-1}, which can be attributed to $C^{\alpha}-C^{\beta}$ stretching of side chains located within α-helical domains (*29*, *30*). These findings are in accord with a previous spectroscopic examination of the polymerase core (*27*). To quantitatively assess the amount of α-helix present in the P1 monomer, we employed a reference profile method (*31*) utilizing the amide I band contour in trace B of Figure 2. This method gives the following estimate of secondary structure: 59 ± 5% α-helix, 17 ± 5% β-strand, and 24 ± 7% disordered structure (i.e., irregular conformations, including loops and turns).

The Raman spectrum of P1 within the PC assembly can be estimated to a first approximation by compensating the Raman spectrum of the P14 particle (Table 1) for contribu-

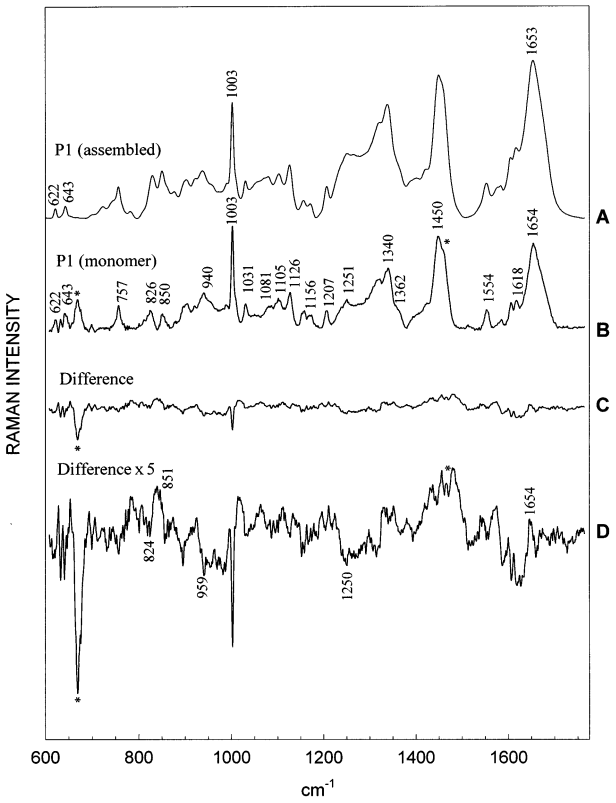

FIGURE 2: Raman signatures of P1 protein in different assembly states. (A) Spectrum of assembled P1 generated by subtraction of the Raman spectrum of the purified P4 hexamer from that of the P14 particle (Table 2), each at 100 μg/μL. (B) P1 monomer at 4 μg/μL in 20 mM Tris (pH 8.1), 0.5 M NaCl. (C) Difference spectrum [A − B] scaled with respect to P1. (D) Magnification (5×) of C. Labels indicate prominent Raman bands discussed in the text, including amide I and amide III secondary structure markers of the monomer and assembly at 1654 and 1251 cm^{-1}, respectively. Asterisks (∗) in the P1 monomer spectrum designate uncompensated bands of the buffer.

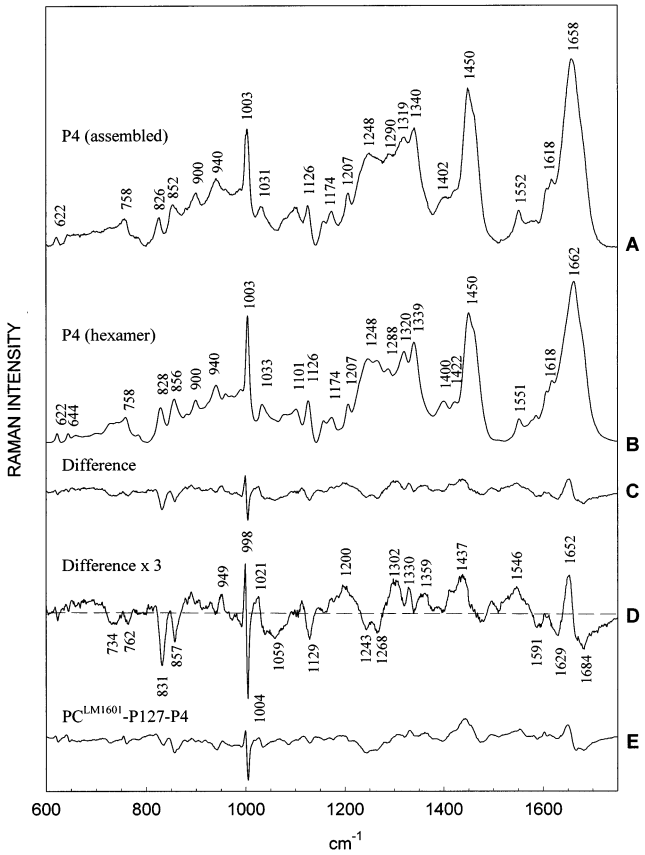

FIGURE 3: Raman spectra of P4 protein in different assembly states. (A) Spectrum of P4 in the procapsid assembly (P4′) generated by subtracting the Raman spectrum of the P127 particle from that of the PC, each at 100 μg/μL. (B) Spectrum of the isolated P4 hexamer at 50 μg/μL. (C) Difference spectrum [A − B] scaled with respect to P4, representing the perturbations to the Raman spectrum of P4 resulting from incorporation in the PC. (D) A 3-fold expansion of the difference spectrum shown in C. (E) Difference PC^{LM1601}−P127−P4 scaled with respect to P4.

tions of the P4 protein. Such a spectral subtraction is shown in Figure 2, trace A. The spectrum of this P1 assembly exhibits an amide I band at 1653 cm^{-1} and an amide III band at 1251 cm^{-1}, indicating a subunit secondary structure very similar to that of the P1 monomer. On the basis of the marginal difference peak at 1654 cm^{-1} and trough at 1250 cm^{-1} in the computed difference spectrum (Figure 2, trace D), a very slight increase in α-helicity at the expense of irregular structure may occur. Thus, PC assembly occurs with at most a marginal ordering of the polypeptide chains of P1 and/or P4.

While the data of Figure 2 indicate that nativelike secondary structure is conserved between the P1 monomer (trace B) and assembly (trace A), many side-chain environments are altered. The environment of the average tyrosine residue is clearly affected, as manifested by the large increase in the ratio of intensities (I_{851}/I_{824}) of tyrosine markers at 851 and 824 cm^{-1} (*32*). Unfortunately, it is not possible to ascribe these differences solely to P1 since, as shown below, P4 also contributes Raman intensity in this region of the spectrum and the structure of P4 within the P14 particle is perturbed by assembly.

Expression of P1 alone in *E. coli* leads to the formation of an inclusion body aggregate (P1^{agg}). The Raman signature of P1^{agg} (not shown) differs significantly from those of the P1 monomer and assembly, consistent with a non-native, off-pathway conformation.

Incorporation of the P4 Hexamer into the Procapsid. Raman Signature and Secondary Structure of the Isolated P4 Hexamer. The Raman spectrum of the purified recombinant P4 hexamer is shown in Figure 3, trace B. This spectrum is virtually identical to the P4 hexamer spectrum reported previously (*25*). Both Raman and CD analyses are consistent with a P4 subunit structure consisting of an α/β fold. The secondary structure estimated by curve fitting (*31*) of the Raman amide I profile of Figure 3B indicates 30 ± 3% α-helix, 28 ± 1% β-strand, and 42 ± 2% irregular structure, in agreement with the previous estimate (*25*).

Raman Signature of P4 in the Procapsid: Evidence for Assembly-Induced Structural Changes. The Raman signature of the P4 hexamer incorporated into the procapsid has been obtained by subtracting the spectrum of the P127 particle from that of the procapsid. The result, shown in Figure 3A, is considered to be a reasonable approximation to the Raman signature of the P4 hexamer in the PC (designated as P4′ in Table 2), even though this difference spectrum includes any spectral changes that might represent attendant structural perturbations to P1, P2, and P7 components of the assembly. However, because P2 and P7 represent only 5.5% and 7%, respectively, of the total PC mass, they are not expected to

make major contributions to either the PC or P127 spectrum. Also, the expected small spectral perturbations of P2 and P7 may be largely compensated by the subtraction. On the other hand, P1 represents 69% of the total PC mass and assembly related changes in P1 may not be entirely compensated by the subtraction yielding Figure 3A. Nevertheless, an approximate structural comparison between the P4 hexamer incorporated into the procapsid and the isolated P4 hexamer can be projected by subtracting the corresponding Raman signatures (Figure 3A,B) from one another. The resulting P4′-minus-P4 difference spectrum is shown in Figure 3C (unamplified) and Figure 3D (amplified 3-fold). The data suggest a striking change in the P4 subunit structure with PC incorporation. The signal-to-noise quality of Figure 3D is remarkable, considering that the trace represents a 3-fold amplification of a second difference spectrum and that no data smoothing of any kind has been employed.

The difference peaks at 1652 and 1302 cm^{-1} in Figure 3D are assigned, respectively, to amide I and amide III modes of excess α-helical secondary structure in P4′, whereas the corresponding troughs at 1668−1684 and 1243 cm^{-1} are assigned to amide I and amide III of irregular structure (*33*, *34*). Fitting the amide I region of the P4′ spectrum using the reference profile method (*31*) yields 44 ± 3% α-helix, 23 ± 1% β-strand, and 33 ± 2% irregular structure. Accordingly, Figure 3D indicates a substantial assembly induced increase in α-helicity (14 ± 6%) of the P4 subunit, primarily at the expense of unordered structure (−9 ± 3%), upon incorporation of the P4 hexamer into the PC. The very rich pattern of additional peaks and troughs (as labeled in Figure 3D) demonstrates that extensive changes also occur in the local environments and interactions of subunit side chains of P4 (i.e., tertiary structure) with PC assembly. The perturbations to Raman markers of tyrosine (831, 857, 1268 cm^{-1}), phenylalanine (998, 1004 cm^{-1}), and tryptophan (1359, 1546 cm^{-1}) are particularly striking. The troughs at 831 and 857 cm^{-1} indicate that the average Tyr phenoxyl group is a much stronger hydrogen bond acceptor in the PC assembly than in the isolated state (*32*). The trough at 1004 and satellites at 998 and 1021 cm^{-1}, which result from an unusually broad Phe marker at 1003 cm^{-1} in the PC assembly, indicate greater heterogeneity of Phe environments in the PC. The peaks at 1359 and 1546 cm^{-1} indicate that the indolyl ring environments are more hydrophobic in the PC (*35*, *36*). The peaks at 949, 1330, and 1437 cm^{-1} and troughs at 1059 and 1129 cm^{-1}, which are due to aliphatic groups of various side chains, indicate that environments of the nonaromatics are also altered significantly by PC assembly (*37*).

Raman spectra were also collected from PC particles generated by use of the LM1601 plasmid. These particles (PC^{LM1601}, see Tables 1 and 2) are partially deficient in P4. As shown in Figure 3 (trace E), the P4 difference spectrum is almost identical to that of the wild-type procapsid when scaled with respect to the amount of P4 in the PC^{LM1601} particle. The results confirm that the magnitude of the observed differences is proportional to the amount of P4 retained in the PC assembly.

Contributions of Minor Proteins P2 and P7 to Procapsid Structure. P2 Polymerase. P2, the φ6 RNA polymerase, was expressed in sufficient quantity for spectroscopic analysis of the monomer (*24*) (Figure 4, middle trace). The amide I

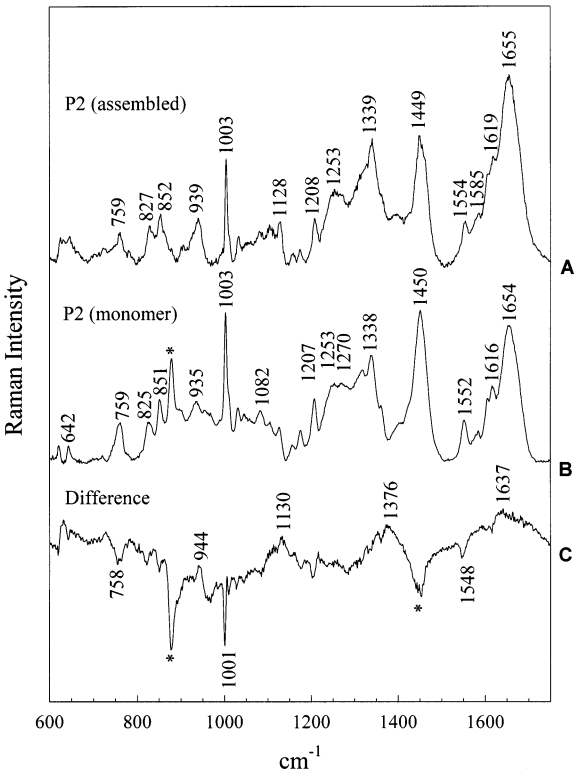

FIGURE 4: Raman spectra of P2 protein in different assembly states. (A) Spectrum of P2 in the procapsid assembly (P2′) generated by subtracting the Raman spectrum of the P147 particle from that of the PC, each at 100 μg/μL. (B) Spectrum of the isolated P2 protein at 50 μg/μL. (C) Difference spectrum [A − B].

maximum at 1654 cm^{-1} is consistent with an α-helical fold in the monomer. This is further supported by the appearance of amide III at 1270 cm^{-1} and a main chain marker at 1338 cm^{-1}. The secondary structure estimated by curve fitting of the Raman amide I profile is 54% α-helix, 23% β-strand, and 23% irregular structure (*31*), which compares favorably with analysis of the crystal structure of P2 (46% α-helix, 13% β-strand, and 41% irregular structure) (*38*).

Obtaining the Raman signature of P2 in procapsid and procapsid-like particles by subtraction methods is subject to large errors, owing to the very low copy number per particle (12 copies or 5.5 wt % of the procapsid). With this limitation in mind, we have estimated the Raman signature of P2 in the assembled PC by subtracting the spectrum of the P147 particle from that of the PC. The result is shown in the top trace of Figure 4. To assess the combined effects of P2 structural changes with assembly and of the structural impact of P2 on other protein components of the PC, a difference spectrum was generated by subtraction of the spectrum of the P2 monomer (Figure 4, middle trace) from the spectral signature of P2 in the assembled state (Figure 4, top trace). This result, which is shown in the bottom trace in Figure 4, exhibits no clear-cut difference bands in either the amide I or amide III regions. The only significant difference bands (excluding very broad features that are likely due to baseline differences) occur in bands of Trp (758, 1548 cm^{-1}) and Phe (1001 cm^{-1}). We conclude that the incorporation of P2 into the PC assembly does not introduce large conformational changes in PC components, although aromatic side-chain environments are altered perceptibly. It should also be noted that the spectrum of the P2 monomer contains buffer

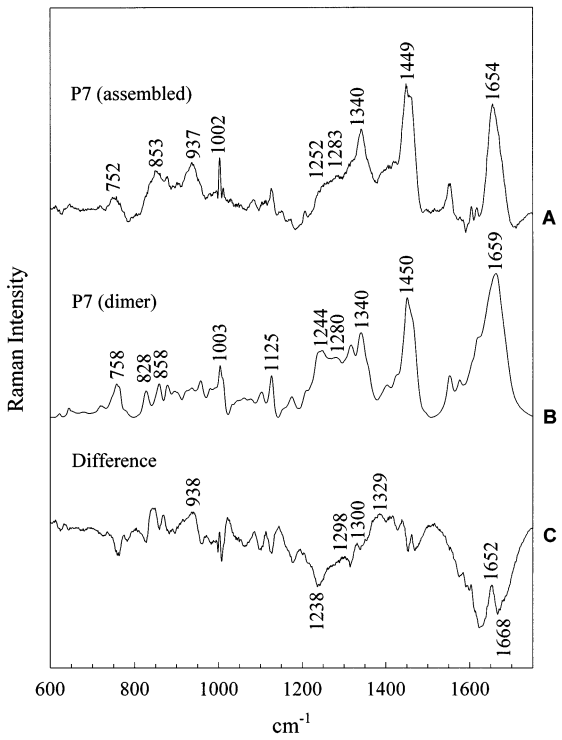

FIGURE 5: Raman spectra of P7 protein in different assembly states. (A) Spectrum of P7 in the procapsid assembly (P7′) generated by subtracting the Raman spectrum of the P124 particle from that of the PC, each at 100 μg/μL. (B) Spectrum of the isolated P7 protein (dimer) at 50 μg/μL. (C) Difference spectrum [A − B].

contributions (Figure 4, middle trace, asterisks) that could not be perfectly compensated in the difference spectrum.

Accessory Protein P7. The Raman spectrum of the purified recombinant P7 dimer is shown in the middle trace of Figure 5. The Raman amide I marker (1659 cm^{-1}) and amide III markers (1244 and 1280 cm^{-1}) indicate that P7 also contains an α/β fold. The secondary structure estimated by curve fitting of the Raman amide I profile is 35% α-helix, 29% β-strand, and 36% irregular structure.

Despite the relatively high copy number of P7 (60) in the PC, the small size of the monomer (17 kDa) is expected to result in relatively large errors in spectral subtractions. An approximation to the Raman signature of P7 incorporated into the PC (Figure 5, top trace) was obtained by subtracting the Raman spectrum of the P124 particle from that of the PC. Comparison in turn with the spectrum of the P7 dimer (Figure 5, middle trace) yields the difference spectrum shown in the bottom trace of Figure 5. Although interpretation of this difference profile is complicated by both a high noise level and a sloping background, the amide I (1688 → 1652 cm^{-1}) and amide III (1238, 1300, 1329 cm^{-1}) difference features, as well as the peak at 938 cm^{-1}, indicate greater α-helicity for P7 of the procapsid. Decomposition of the amide I changes using the reference profile method (*31*) yields an estimate of 20 ± 6% more α-helix in the assembled state of the P7 subunit. This finding is similar to that obtained for P4.

Exogenous RNA Binding to Procapsid-Like Particles. Raman spectroscopy reveals nonspecific binding of RNA to the P124 particle (data not shown). The bound RNA was eliminated by extensive RNase treatment prior to the final purification procedure. Interestingly, the full PC and all other procapsid-like assemblies were isolated without bound RNA, irrespective of RNase treatment. This suggests that the absence of P7 in the P124 particle exposes RNA-binding sites within or on the surface of the P124 assembly.

DISCUSSION

Roles of P1 and P4 in Procapsid Assembly. Our results demonstrate that interactions between P1 and P4 subunits are important for correct procapsid assembly. Binding of the P4 hexamer within the P14 particle induces ordering of the polypeptide main chains (increase in α-helix) as well as changes in local environments of side chains (e.g., increase in Trp hydrophobicity). Such ordering of the polypeptide backbone and increased hydrophobicity of Trp side chains are consistent with assembly induced local folding in the P1 and P4 main chains and sequestration of their side chains at subunit interfaces.

A second and independent line of evidence that the P1/P4 interaction provides the key stabilizing force for correct procapsid assembly is provided by the PC^{LM1601} construct (Table 1), which incorporates less than stoichiometric amounts of P4. In PC^{LM1601} particles, the Raman amide band differences—and therefore the secondary structure perturbations—are proportional to P4 content (Figure 3). This implies that reordering of P1 secondary structure is related directly to the extent of P1/P4 interaction. Further assignment of the observed structural changes to particular subunit domains or local sequences in P1 or P4 is beyond the currently employed methods, although isotope-edited Raman spectroscopy could be used to address such questions.

It is interesting that mutational analyses of P4 support the present spectroscopic results. For example, the C-terminal 13 amino acids of P4 are essential for incorporation into the PC but are not required for oligomerization or NTPase activity (*23*). About 40 residues at the C-terminus of P4 are also prone to proteolytic cleavage (J. Juuti, M. Pirttimaa & D. Bamford, unpublished results, 2002) and are probably disordered. Accordingly, the C-terminal segment of P4 is the likely candidate for the secondary structure changes shown by Raman difference spectroscopy to represent ordering of roughly 40−50 residues.

The expression of P1 in the absence of P4 or P7 results in the formation of an inclusion body aggregate (*23*). The $P1^{agg}$ spectrum (not shown) implies appreciable loss of native α-helical secondary structure in the aggregated form. This is consistent with the notion that interactions of P1 with P4 and P7 not only induce α-helix formation in the latter proteins but also stabilize the native P1-fold. In the absence of such stabilizing effects, local unfolding presumably ensues, followed by the formation of intermolecular β-strands and aberrant particle formation.

The strong assembly-related interactions and polypeptide chain refolding proposed for P1 and P4 are similar to the assembly induced refolding observed in the icosahedral dsDNA viruses, P22 and PRD1 (*17*, *19*). The concept of assembly induced folding is consistent with a recent in vitro study in which it was shown that the P4 hexamer is essential for nucleation of the properly dimensioned and biologically active PC assembly (*6*). Because protein P1 does not dimerize spontaneously, the P4 hexameric ring may promote an initial P1 dimerization step. This is indicated schematically in

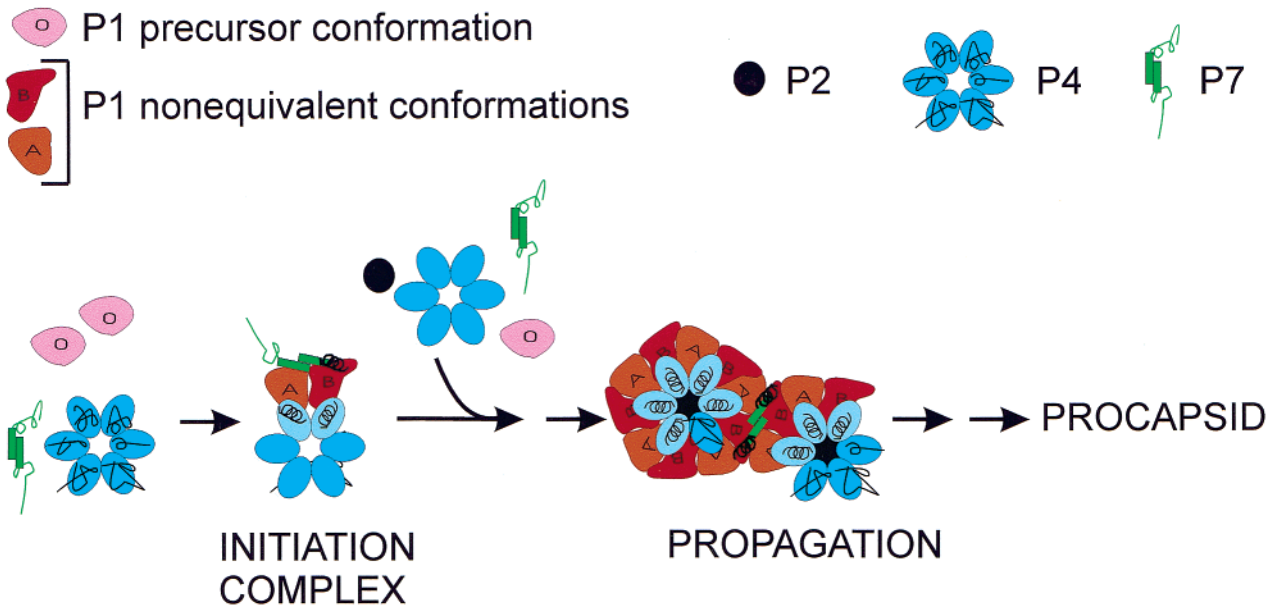

FIGURE 6: Conformational changes mapped onto the assembly pathway of the φ6 procapsid (*6*). Three conformational variants are proposed for P1, including a monomeric precursor (O, pink) and two mature conformations (A, orange; B, red) comprising a nonsymmetrical dimer. The initiation complex involves interaction of the A/B hetero dimer with a P4 hexamer (blue), leading to folding of disordered regions into α-helical structure (light blue subunits). Similarly, a disordered domain (green) of the P7 dimer becomes ordered (black helices) upon stabilization of the 2-fold contacts between P1 molecules. The P2 monomer (black) is incorporated at each 5-fold vertex without substantial conformational change. In subsequent steps the building blocks are added following the same conformational changes as those in the initiation step. Note that differential folding of P4 subunits within the procapsid provides a simple way to accommodate the symmetry mismatch at the 5-fold vertexes.

Figure 6. Although P1 can form assemblies in the absence of P4 (e.g., when expressed in *E. coli* as the P127 particle), the particles so formed are metastable and ultimately produce aberrant aggregates (*23*). Thus, P4 may be required not only to nucleate PC assembly but also to stabilize the correct assembly architecture.

The symmetry mismatch demonstrated between the P1 decamer and P4 hexamer (*12*) may result from steric hindrance imposed by packing of P1. This mismatch ultimately leads to nonequivalent contacts between P1 and P4. Such contacts may be accommodated by variations in local folding, as the present results suggest. A corresponding type of symmetry mismatch has also been proposed for the portal proteins of dsDNA phages (*39*).

Role of P7 in Procapsid Assembly. Although P7 is a minor component of the PC, structural changes stemming from the binding of P7 within the PC (Figure 5) appear to be comparable to those assigned to the interaction between P1 and P4 (Figure 3). Conversely, changes in subunit main chain conformation are negligible with P2 incorporation (Figure 4), despite the fact that P2 and P7 contribute roughly equally to the total protein mass of the PC. Because P7 does not interact with P4 in the core particle (*8*, and unpublished results of R. Tuma), the observed conformational change is most likely due to direct P1/P7 association. Preliminary NMR and solution X-ray scattering data (S. Butcher, R. Tuma & D. Bamford, unpublished results, 2002) indicate that the C-terminal portion of the P7 dimer is disordered. This further suggests that P1/P7 interaction leads to ordering of an extended conformation upon assembly.

Previously, it was shown that P7 accelerates assembly in vitro (*6*). As noted above, the elongated P7 dimer may act as a clamp across the 2-fold axis of the dodecahedron to stabilize decamer−decamer contacts during assembly (Figure 6). Such P1/P7 interactions could provide stabilization complementary to that provided by P1/P4 contacts near the 5-fold vertexes. The compromised stability of the P124 particle may account for defects in packaging and RNA +strand synthesis (*8*, *21*). In this regard, P7 may be analogous to the Sid scaffolding protein of bacteriophage P4 (*40*) and surface glue proteins of other viruses.

CONCLUSIONS

Raman spectroscopy has been used to characterize structural changes attendant with assembly of the polymerase complex of the dsRNA virus φ6. The present study, which relies on a combination of genetic and spectroscopic approaches, allows comparison of conformational structures of protein constituents of the φ6 procapsid in unassembled, partially assembled and fully assembled states. Two key interactions between procapsid proteins have been identified, namely P1/P4 and P1/P7. These interactions are essential for the nucleation of assembly (P1/P4) and stabilization of the 2-fold contacts (P1/P7) at solution concentrations approximating those in vivo. The P1/P4 and P1/P7 interactions induce local folding of polypeptide chains during assembly in a fashion similar to that observed for bacteriophages P22 (*19*), PRD1 (*17*), and MS2 (*41*).

ACKNOWLEDGMENT

We thank Dr. Eugeny Makeyev for providing purified P2 protein and pEM1 plasmid and Drs. Minna Poranen and Tero Viitanen for assistance with P1 expression and purification.

REFERENCES

1. Grimes, J. M., Burroughs, J. N., Gouet, P., Diprose, J. M., Malby, R., Zientara, S., Mertens, P. P., and Stuart, D. I. (1998) The atomic structure of the blue tongue virus core, *Nature 395*, 470−478.

2. Mindich, L., and Bamford, D. H. (1988) Lipid-containing Bacteriophages, in *The Bacteriophages* (Calendar, R., Ed.) Vol. 2, pp 475−520, Plenum Press, New York.
3. Olkkonen, V. M., Gottlieb, P., Strassman, J., Qiao, X. Y., Bamford, D. H., and Mindich, L. (1990) *In vitro* assembly of infectious nucleocapsids of bacteriophage φ6: Formation of a recombinant double-stranded RNA virus, *Proc. Natl. Acad. Sci. U.S.A. 87*, 9173−77.
4. Reinisch, K. M., Nibert, M. L., and Harrison, S. C. (2000) Structure of the reovirus core at 3.6 Å resolution, *Nature 404*, 960−967.
5. Bamford, D. H. (2000) Virus structures: those magnificent molecular machines, *Curr. Biol. 10*, R558−R561.
6. Poranen, M. M., Paatero, A. O., Tuma, R., and Bamford, D. H. (2001) Self-assembly of a viral molecular machine from purified protein and RNA constituents, *Mol. Cell 7*, 845−854.
7. Butcher, S. J., Dokland, T., Ojala, P. M., Bamford, D. H., and Fuller, S. D. (1997) Intermediates in the assembly pathway of the double-stranded RNA virus φ6, *EMBO J. 16*, 4477−4487.
8. Juuti, J. T., and Bamford, D. H. (1997) Protein P7 of phage φ6 RNA polymerase complex, acquiring of RNA packaging activity by *in vitro* assembly of the purified protein onto deficient particles, *J. Mol. Biol. 266*, 891−900.
9. Koonin, E. V., Gorbalenya, A. E., and Chumakov, K. M. (1989) Tentative identification of RNA-dependent RNA polymerases of dsRNA viruses and their relationship to positive strand RNA viral polymerases, *FEBS Lett. 252*, 42−46.
10. Bamford, D. H., Romantschuk, M., and Somerharju, P. J. (1987) Membrane fusion in prokaryotes: bacteriophage φ6 membrane fuses with the *Pseudomonas syringae* outer membrane, *EMBO J. 6*, 1467−1473.
11. Kenney, J. M., Hantula, J., Fuller, S. D., Mindich, L., Ojala, P. M., and Bamford, D. H. (1992) Bacteriophage φ6 envelope elucidated by chemical cross-linking, immunodetection, and cryoelectron microscopy, *Virology 190*, 635−644.
12. Poranen, M. M., Daugelavicius, R., Ojala, P. M., Hess, M. W., and Bamford, D. H. (1999) A novel virus-host cell membrane interaction. Membrane voltage-dependent endocytic-like entry of bacteriophage φ6 nucleocapsid, *J. Cell. Biol. 147*, 671−682.
13. Tuma, R., Bamford, J. K. H., Bamford, D. H., and Thomas, G. J, Jr. (1999) Assembly dynamics of the nucleocapsid shell subunit (P8) of bacteriophage φ6, *Biochemistry 38*, 15025−15033.
14. de Haas, F., Paatero, A. O., Mindich, L., Bamford, D. H., and Fuller, S. D. (1999) A symmetry mismatch at the site of RNA packaging in the polymerase complex of dsRNA bacteriophage φ6, *J. Mol. Biol. 294*, 357−372.
15. Gottlieb, P., Strassman, J., Qiao, X. Y., Frucht, A., and Mindich, L. (1990) *In vitro* replication, packaging, and transcription of the segmented double-stranded RNA genome of bacteriophage φ6: Studies with procapsids assembled from plasmid-encoded proteins, *J. Bacteriol. 172*, 5774−5782.
16. Thomas, G. J., Jr. (1999) Raman spectroscopy of protein and nucleic acid assemblies, *Annu. Rev. Biophys. Biomol. Struct. 28*, 1−27.
17. Tuma, R., Bamford, J. K. H., Bamford, D. H., Russell, M. P., and Thomas, G. J., Jr. (1996) Structure, interactions and dynamics of PRD1 virus. I. Coupling of subunit folding and capsid assembly, *J. Mol. Biol. 257*, 87−101.
18. Tuma, R., Prevelige, P. E., Jr., and Thomas, G. J., Jr. (1998) Mechanism of capsid maturation in a double-stranded DNA virus, *Proc. Natl. Acad. Sci. U.S.A. 95*, 9885−9890.
19. Tuma, R., Tsuruta, H., Prevelige, P. E., Jr., and Thomas, G. J., Jr. (2001) Structural changes during assembly of bacteriophage P22, *Biochemistry 40*, 665−674.
20. Raso, S. W., Clark, P. L., Haase-Pettingell, C., King, J., and Thomas, G. J., Jr. (2001) Distinct cysteine sulfhydryl environments detected by analysis of Raman S−H markers of Cys → Ser mutant proteins, *J. Mol. Biol. 307*, 899−911.
21. Juuti, J. T., and Bamford, D. H. (1995) RNA binding, packaging and polymerase activities of the different incomplete polymerase complex particles of dsRNA bacteriophage φ6, *J. Mol. Biol. 249*, 545−554.
22. Benevides, J. M., Wang, A. H.-J., van der Marel, G. A., van Boom, J. H., Rich, A., and Thomas, G. J., Jr. (1984) The Raman spectra of left-handed DNA oligomers incorporating adenine-thymine base pairs, *Nucleic Acids Res. 12*, 5913−5925.
23. Paatero, A. O., Mindich, L., and Bamford, D. H. (1998) Mutational analysis of the role of nucleoside triphosphatase P4 in the assembly of the RNA polymerase complex of bacteriophage φ6, *J. Virol. 72*, 10058−10065.
24. Makeyev, E. V., and Bamford, D. H. (2000) Replicase activity of purified recombinant protein P2 of double-stranded RNA bacteriophage φ6, *EMBO J. 19*, 124−133.
25. Juuti, J. T., Bamford, D. H., Tuma, R., and Thomas, G. J., Jr. (1998) Structure and NTPase activity of the RNA-translocating protein (P4) of bacteriophage φ6, *J. Mol. Biol. 279*, 347−359.
26. Caldentey, J., Tuma, R., and Bamford, D. H. (2000) Assembly of bacteriophage PRD1 spike complex: Role of the multidomain protein P5, *Biochemistry 39*, 10566−10573.
27. Bamford, J. K. H., Bamford, D. H., Li, T., and Thomas, G. J., Jr. (1993) Structural studies of the enveloped dsRNA bacteriophage φ6 of *Pseudomonas syringae* by Raman spectroscopy. II. Nucleocapsid structure and thermostability of the virion, nucleocapsid and polymerase complex, *J. Mol. Biol. 230*, 473−482.
28. Li, T., Bamford, D. H., Bamford, J. K. H., and Thomas, G. J., Jr. (1993) Structural studies of the enveloped dsRNA bacteriophage φ6 of *Pseudomonas syringae* by Raman spectroscopy. I. The virion and its membrane envelope, *J. Mol. Biol. 230*, 461−472.
29. Tuma, R., Prevelige, P. E., Jr., and Thomas, G. J., Jr. (1996) Structural transitions in the scaffolding and coat proteins of P22 virus during assembly and disassembly, *Biochemistry 35*, 4619−4627.
30. Bandekar, J. (1992) Amide modes and protein conformation, *Biochim. Biophys. Acta 1120*, 123−143.
31. Berjot, M., Marx, J., and Alix, A. J. P. (1987) Determination of the secondary structure of proteins from the Raman amide I band: The reference intensity profiles method, *J. Raman Spectrosc. 18*, 289−300.
32. Siamwiza, M. N., Lord, R. C., Chen, M. C., Takamatsu, T., Harada, I., Matsuura, H., and Shimanouchi, T. (1975) Interpretation of the doublet at 850 and 830 cm^{-1} in the Raman spectra of tyrosyl residues in proteins and certain model compounds, *Biochemistry 14*, 4870−4876.
33. Chen, M. C., and Lord, R. C. (1974) Laser-excited Raman spectroscopy of biomolecules. VI. Some peptides as conformational models, *J. Am. Chem. Soc. 96*, 4750−4752.
34. Chen, M. C., Lord, R. C., and Mendelsohn, R. (1974) Laser-excited Raman spectroscopy of biomolecules. V. Conformational changes associated with the chemical denaturation of lysozyme, *J. Am. Chem. Soc. 96*, 3038−3042.
35. Miura, T., Takeuchi, H., and Harada, I. (1988) Characterization of individual tryptophan side chains in proteins using Raman spectroscopy and hydrogen−deuterium exchange kinetics, *Biochemistry 27*, 88−94.
36. Miura, T., Takeuchi, H., and Harada, I. (1989) Tryptophan Raman bands sensitive to hydrogen bonding and side-chain conformation, *J. Raman Spectrosc. 20*, 667−671.
37. Overman, S. A., and Thomas, G. J., Jr. (1999) Raman markers of nonaromatic side chains in an α-helix assembly: Ala, Asp, Glu, Gly, Ile, Leu, Lys, Ser, and Val residues of phage fd subunits, *Biochemistry 38*, 4018−4027.
38. Butcher, S. J., Grimes, J. M., Makeyev, E. V., Bamford, D. H., and Stuart, D. I. (2001) A mechanism for initiating RNA-dependent RNA polymerization, *Nature 410*, 235−240.
39. Hendrix, R. W. (1978) Symmetry mismatch and DNA packaging in large bacteriophages, *Proc. Natl. Acad. Sci. U.S.A. 75*, 4779−4783.
40. Marvik, O. J., Dokland, T., Nokling, R. H., Jacobsen, E., Larsen, T., and Lindqvist, B. H. (1995) The capsid size-determining protein Sid forms an external scaffold on phage P4 procapsids, *J. Mol. Biol. 251*, 59−75.
41. Ni, C. Z., Syed, R., Kodandapani, R., Wickersham, J., Peabody, D. S., and Ely, K. R. (1995) Crystal structure of the MS2 coat protein dimer: Implications for RNA binding and virus assembly, *Structure 3*, 255−263.
42. Ojala, P. M., Juuti, J. T., and Bamford, D. H. (1993) Protein P4 of double-stranded RNA bacteriophage φ6 is accessible on the nucleocapsid surface: Epitope mapping and orientation of the protein, *J. Virol. 67*, 2879−2886.

BI0201623